An Effective Near-Field Far-Field Transformation Technique from Truncated and Inaccurate Amplitude-Only Data

Ovidio M. Bucci, *Fellow, IEEE*, Giuseppe D'Elia, and Marco Donald Migliore

***Abstract*—A general approach to the near-field far-field transformation from amplitude only near-field data is presented. The estimation of the far field is stated as an intersection finding problem and is solved by the minimization of a suitable functional. The difficulties related to the possible trapping of the algorithm by a false solution (common to any nonlinear inverse problem) are mitigated by setting the problem in the space of the squared field amplitudes (as already done in a number of existing papers) and by incorporating all the *a priori* knowledge concerning the system under test in the formulation of the problem. Accordingly, the *a priori* information concerning the far field, the near field outside the measurement region and the accuracy of the measurement setup and its dynamic range are properly taken into account in the objective functional. The intrinsic ill conditioning of the problem is managed by adopting a general, flexible, and nonredundant sampling representation of the field, which takes into account the geometrical characteristics of the source. As a consequence, the number of unknowns is minimized and a technique is obtained, which easily matches the available knowledge concerning the behavior of the field. The effectiveness of the approach is shown by reporting the main results of an extensive numerical analysis, as well as an experimental validation performed by using a very low cost near-field facility available at the Electronic Engineering Department, University of Napoli, Italy.**

***Index Terms*—Near-field far-field transformation, only amplitude measurement.**

I. Introduction

THE evaluation of the radiation pattern of an antenna from near-field measurements by means of a near-field far-field (NF–FF) transformation is a well established and widely used technique [1]–[3] that has been applied by exploiting several scanning geometries, including recent bipolar and spiral geometries [4]–[6]. All standard NF–FF transformation algorithms need an accurate knowledge of the near-field phase. However, the measurement of the near-field phase with the accuracy required to obtain a reliable far-field reconstruction becomes increasingly difficult and expensive when the working frequency increases up to the millimeter range, thus requiring either very sophisticated apparatuses or special means such as interferometric techniques [7].

In order to avoid any phase measurement, approaches based on the measurement of the near-field amplitude on two (or more) near-zone surfaces have been proposed [8]–[12]. The main drawback of all amplitude only approaches is related to the fact that they essentially rely on the retrieval of the phase of the measured field and therefore involves the solution of a nonlinear inverse problem. Because the phase retrieval problem is ill posed [13], [14], so too is the far-field determination from (truncated and noise corrupted) near-field intensity data: thus, we can only look for a generalized solution by minimizing a suitable functional, which also acts as a stabilizing functional.

However, because of the nonconvex nature of the problem, the objective functional usually exhibits many local minima so that the solution algorithm can be trapped in a false solution, thus making the corresponding NF–FF transformation technique unreliable. To deal with this difficulty, the following points should be taken into account.

1) A suitable *mathematical formulation* of the problem should be adopted in order to simplify, as much as possible, the kind of nonlinearity to be handled.
2) A nonredundant field representation should be exploited in order to reduce, as much as possible, the *number of unknowns* that strongly affect both the ill conditioning of the problem and the number of traps.
3) All the available *a priori* information concerning the far-field, the near-field outside the measurement region, the shape of the antenna under test, and the accuracy of the measurement setup and its dynamic range should be taken into account. As a matter of fact, the full exploitation of available *a priori* information, which amounts to reducing the effective number of unknowns, should be considered as relevant as the measurements themselves and is a key tool for managing ill conditioning and trapping problems.

It is worth noting that the fulfillment of above points, in general does not lead to a convex objective functional. Accordingly, the local minima problem, although alleviated and handled at the "best," cannot be completely avoided unless global minimization procedures (such as simulated annealing or genetic algorithms [15]–[17]), which are very heavy from the computational point of view, are adopted.

Recently, a new convenient formulation has been introduced which answers points 1) and 2) in the case of aperture antennas [12]. It reduces the nonlinearity of the problem to a quadratic one, i.e., the simplest possible one, and drastically reduces

Manuscript received February 23, 1998; revised January 4, 1999.

The authors are with the Dipartimento di Ingegneria Elettronica e delle Telecomunicazioni, Università di Napoli "Federico II," Napoli, 80125 Italy.

Publisher Item Identifier S 0018-926X(99)07062-3.

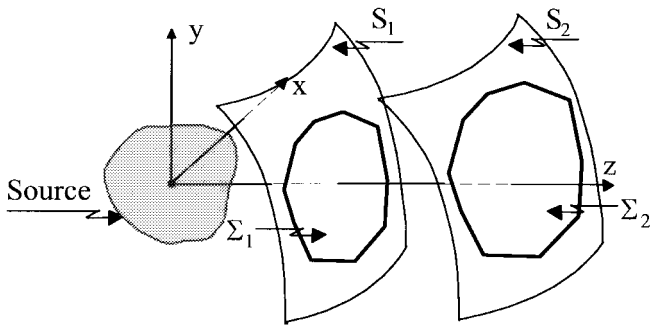

Fig. 1. Geometry of the problem.

the occurrence of false solutions, thus providing a reliable transformation technique.

However, the approach does not exploit any *a priori* information on the near-field and on the accuracy and dynamic range of the measurement system and, despite being well suited to the case of focusing aperture antennas, does not deal with more general classes of antennas.

In this paper we introduce an amplitude-only NF–FF transformation technique, which attempts to take into account, in a general way, all the points outlined before. The technique is based on an intersection finding approach, which is reduced to the minimization of a suitable objective functional.

As far as point 1) is concerned, following [12], the approach presented here involves a quadratic inverse problem.

Concerning point 2), a nonredundant and effective representation of the field radiated on an arbitrary surface by a generic source of given geometrical characteristics is exploited [18], [19].

Point 3) is answered by suitably defining the sets involved and, thus, the goal functional to be minimized.

The mathematical statement of the problem and the solution algorithm are presented in Section II. The nonredundant field representation exploited in the approach is briefly outlined in Section III. Some examples of an extensive numerical analysis showing the effectiveness of the technique presented are reported in Section IV. The results obtained by exploiting the experimental data collected by the low-cost facility available in our Department are also shown in this section and the conclusions are given in Section V.

II. Statement of the Problem and Solution Algorithm

As stated before, our goal is to determine the far-field pattern of an arbitrary source S from (incomplete and noisy) near-field amplitude measurements on two scanning surfaces, say S_1 and S_2 (see Fig. 1). To manage the ill conditioning of the problem and the occurrence of false solutions all points outlined in the Introduction must be taken into account when developing a general and effective NF–FF transformation algorithm.

As far as the mathematical setting of the problem is concerned, a new formulation has been recently introduced into the field of phase retrieval and antenna synthesis problems. It adopts an intersection finding approach in the space of the semi-definite positive functions associated to the squared amplitude of the fields [12]. In this way, a quadratic relationship between the unknowns and the measured quantities is exploited, thus reducing the nonlinearity of the problem to the simplest possible one. The quartic nature of the objective functional corresponding to this choice makes it possible to effectively control and reduce the occurrence of false solutions. According to these results, in this paper, the far-field pattern determination from near-field amplitude data is stated by making reference to the squared amplitude of the measured fields and by referring suitable sets in the space of the semi-definite positive, square integrable, functions.

Let us assume that the field measurements provide the corrupted squared amplitudes $\widehat{M}^2_{1\mathrm{co}}$, $\widehat{M}^2_{2\mathrm{co}}$, and $\widehat{M}^2_{1\mathrm{cr}}$, $\widehat{M}^2_{2\mathrm{cr}}$ of the copolar field components $M^2_{1\mathrm{co}}$, $M^2_{2\mathrm{co}}$ and the cross-polar ones $M^2_{1\mathrm{cr}}$, $M^2_{2\mathrm{cr}}$, radiated by the source on the regions Σ_1, and Σ_2 of S_1 and S_2, respectively (Fig. 1), and let us define the vectors $\underline{M}^2_1 = (M^2_{1\mathrm{co}}, M^2_{1\mathrm{cr}})$ and $\underline{M}^2_2 = (M^2_{2\mathrm{co}}, M^2_{2\mathrm{cr}})$.[1] Similarly, let us indicate with $\underline{M}^2_\infty = (M^2_{\infty\mathrm{co}}, M^2_{\infty\mathrm{cr}})$ the vector of the radiated far-field copolar and cross-polar patterns. Let us assume that noise and systematic measurement errors are described by means of additive error terms whose upper bounds on Σ_1 and Σ_2 are given by ε_1 and ε_2, respectively, which can depend on the position of the measurement point. Furthermore, let us suppose that the dynamic range of the measurement system is known and equal to dr (in decibels).

Let us further suppose that some *a priori* knowledge concerning the behavior of the near-field intensity outside Σ_1 and Σ_2 is available; for instance, it may involve the radiated power or the decreasing rate of the radiated power density outside such regions.

Similarly, we assume that some *a priori* knowledge of the radiated far-field power pattern is available; for instance, regarding the focusing nature of the antenna or the decreasing rate of the far-field pattern envelope outside a given angular region, let us say Σ_∞.

Finally, we assume that the "status" of the radiated field is described within a given representation error (which must be suitably smaller than that of the measurement) by means of a "status vector" $\underline{x} \in C^N$.[2] The vector $\underline{x}$, which is our unknown, makes it possible to evaluate the field on the measurement surfaces as well as on the far-zone sphere. In particula,r $\underline{M}^2_1$, $\underline{M}^2_2$, and $\underline{M}^2_\infty$ are given by $\underline{M}^2_1 = \underline{\mathcal{T}}_1(\underline{x})$, $\underline{M}^2_2 = \underline{\mathcal{T}}_2(\underline{x})$, and $\underline{M}^2_\infty = \underline{\mathcal{T}}_\infty(\underline{x})$, respectively, where $\underline{\mathcal{T}}_1$, $\underline{\mathcal{T}}_2$, and $\underline{\mathcal{T}}_\infty$ are known continuous quadratic matricial operators. To be feasible, the amplitude only approach obviously requires that the relationship $x \rightarrow (\underline{M}^2_1, \underline{M}^2_2)$ must be one to one. This point is discussed in [12] and [20], wherein the field spectrum samples are exploited as unknowns and the uniqueness of the solution is reported. By paralleling the reasoning made in [12], it can be shown that also in the more general case considered here the uniqueness of the solution holds, i.e., the relationship between state vector and squared amplitudes on the measuring surfaces is one to one.

[1] For the sake of simplicity, we consider the case of an ideal probe. However, all the formulation can be easily adapted, without any significant modification, to the case of nonideal probes.

[2] This is always possible, because the set of all fields radiated by uniformly bounded sources is compact [22].

Let us now denote by $\mathcal{M}_1$ the set of all vectors $\underline{y}_1 = (y_{1\mathrm{co}}, y_{1\mathrm{cr}})$ whose components are semi-definite positive functions complying with the known behavior of the radiated near-field outside Σ_1 and with the measured data inside Σ_1, i.e., such that

$$\widehat{M}^2_{1\mathrm{co}} - \varepsilon_1 \le y_{1\mathrm{co}} \le \widehat{M}^2_{1\mathrm{co}} + \varepsilon_1 \left(\widehat{M}^2_{1\mathrm{cr}} - \varepsilon_1 \le y_{1\mathrm{cr}} \le \widehat{M}^2_{1\mathrm{cr}} + \varepsilon_1\right)$$

at points of Σ_1 where the inequality

$$[\max(\hat{M}_{1\mathrm{co}})]_{\mathrm{dB}} - [y_{1\mathrm{co}}]_{\mathrm{dB}} < dr \left([\max(\hat{M}_{1\mathrm{cr}})]_{\mathrm{dB}} - [y_{1\mathrm{cr}}]_{\mathrm{dB}} < dr\right)$$

is satisfied and such that

$$y_{1\mathrm{co}} \le 10^{-dr/10} \left(y_{1\mathrm{cr}} \le 10^{-dr/10}\right)$$

at all the remaining points of Σ_1. Let us define (in a similar way) the set $\mathcal{M}_2$ related to the amplitudes of the components of the field radiated on the measurement surface S_2.

Finally, let us denote by $\mathcal{M}_\infty$ the set of all vectors, $\underline{y}_\infty = (y_{\infty\mathrm{co}}, y_{\infty\mathrm{cr}})$ whose components are semi-definite positive functions complying with the known behavior of the radiated far field outside Σ_∞.

In the following, it is assumed that $\mathcal{M}_1$, $\mathcal{M}_2$, and $\mathcal{M}_\infty$ belong to $\mathcal{L}^2 \times \mathcal{L}^2$ wherein $\mathcal{L}^2$ denotes the set of functions square integrable over the corresponding domain, equipped with a proper (possibly weighted) mean-square norm. Note that these sets are closed and *convex*, which strongly help to reduce the occurrence of false solutions.

The determination of the far-field from the near-field data makes it possible to find a point of the intersection $\underline{\mathcal{T}}_1^{-1}(\mathcal{M}_1) \cap \underline{\mathcal{T}}_2^{-1}(\mathcal{M}_2) \cap \underline{\mathcal{T}}_\infty^{-1}(\mathcal{M}_\infty)$, i.e., a point $\underline{x} \in C^N$ such that $\underline{\mathcal{T}}_1(\underline{x}) \in \mathcal{M}_1$, $\underline{\mathcal{T}}_2(\underline{x}) \in \mathcal{M}_2$, and $\underline{\mathcal{T}}_\infty(\underline{x}) \in \mathcal{M}_\infty$ or, equivalently (because $\mathcal{M}_1$, $\mathcal{M}_2$, and $\mathcal{M}_\infty$ are closed), such that

$$d^2(\underline{\mathcal{T}}_1(\underline{x}), \mathcal{M}_1) + d^2(\underline{\mathcal{T}}_2(\underline{x}), \mathcal{M}_2) + d^2(\underline{\mathcal{T}}_\infty(\underline{x}), \mathcal{M}_\infty) = 0 \tag{1}$$

where $d^2(y, \mathcal{A})$ denotes the distance between y and the set $\mathcal{A}$ (in the corresponding space). By denoting by P_1, P_2, and P_∞ the metric projectors onto the sets $\mathcal{M}_1$, $\mathcal{M}_2$, and $\mathcal{M}_\infty$, respectively, the determination of $\underline{x}$ is equivalent to the minimization of the functional

$$\Phi(\underline{x}) = \|\underline{\mathcal{T}}_1(\underline{x}) - P_1\underline{\mathcal{T}}_1(\underline{x})\|^2 + \|\underline{\mathcal{T}}_2(\underline{x}) - P_2\underline{\mathcal{T}}_2(\underline{x})\|^2 + \underline{\mathcal{T}}_\infty(\underline{x}) - P_\infty\underline{\mathcal{T}}_\infty(\underline{x})\|^2 \tag{2}$$

with $\underline{x} \in C^N$, where $\|\cdot\|$ denotes the norm in the corresponding spaces.

As shown in [21] under a more general setting, the properties of the finite-dimensional operator $\mathcal{T} : \underline{x} \to (\underline{\mathcal{T}}_1(\underline{x}), \underline{\mathcal{T}}_2(\underline{x}))$ (continuity and single valuedeness) and the boundness of the sets $\mathcal{M}_1$ and $\mathcal{M}_2$ ensure that the variational problem (2) is strongly well-posed, i.e., any minimizing sequence either converges to a minimum point or contains a converging subsequence.

Under the obvious assumption that the *a priori* information is correct, the sets $\mathcal{M}_1$, $\mathcal{M}_2$, and $\mathcal{M}_\infty$ admit at least one intersection point which correspond to a global minimum of the functional Φ. Usually the intersection set has a finite dimension so that an infinite number of solutions do exist. However, this kind of nonuniqueness is not a drawback and is a direct consequence of the uncertainty of the data. In fact, all these solutions give estimations of the unknowns, which are equivalent within the accuracy allowed by the available *a priori* information and measurement accuracy. However, as already stressed, when the minimization of Φ is performed by a deterministic local optimization scheme, the algorithm can be trapped by local minima of the object functional. The formulation introduced in this paper attempts to reduce the occurrence of such trapping by exploiting all the available *a priori* information as much as possible. As stated before, a further improvement could be the exploitation of a global optimization scheme based on modern evolutionary algorithms as those suggested in [17] in the framework of reflector antenna diagnosis problem.

The minimization of the functional (2) is a particular case of that considered in [21]. By defining the functional

$$\mathcal{N}(\underline{x}, \underline{y}_1, \underline{y}_2, \underline{y}_\infty) = \|\underline{\mathcal{T}}_1(\underline{x}) - \underline{y}_1\|^2 + \|\underline{\mathcal{T}}_2(\underline{x}) - \underline{y}_2\|^2 + \|\underline{\mathcal{T}}_\infty(\underline{x}) - \underline{y}_\infty\|^2 \tag{3}$$

the minimization of (2) can be performed by means of the following iterative algorithm:

$$\underline{y}_1^{(k)} = P_1\underline{\mathcal{T}}_1\left(\underline{x}^{(k)}\right) \tag{4a}$$

$$\underline{y}_2^{(k)} = P_2\underline{\mathcal{T}}_2\left(\underline{x}^{(k)}\right) \tag{4b}$$

$$\underline{y}_\infty^{(k)} = P_\infty\underline{\mathcal{T}}_\infty\left(\underline{x}^{(k)}\right) \tag{4c}$$

$$\underline{x}^{(k+1)} : \mathcal{N}\left(\underline{x}^{(k+1)}, \underline{y}_1^{(k)}, \underline{y}_2^{(k)}, \underline{y}_\infty^{(k)}\right) = \min_{\underline{x} \in C^N} \mathcal{N}\left(\underline{x}, \underline{y}_1^{(k)}, \underline{y}_2^{(k)}, \underline{y}_\infty^{(k)}\right) \tag{4d}$$

where $\underline{x}^{(k)}$ is the value of $\underline{x}$ obtained at the kth iteration step. As shown in [21], the algorithm (4a)–(4d) provides a minimizing sequence Φ, which conveys to the solution when Φ has a unique minimum.

The projectors P_1, P_2, and P_∞ can easily be evaluated for most cases of interest (see Appendix).

It must be noted that apart from such examples, other *a priori* information on the near-field (or the far-field) could be incorporated in the technique. To this end, it is only required that a suitable set of near (or far-field) amplitudes, corresponding to the *a priori* information, can be defined and that the projectors on such set can be explicitly evaluated.

Concerning the development of step (4d) it is worth noting that to obtain a minimizing sequence $\{\underline{x}^{(k)}\}$ it is not really necessary to reach the minimum value of $\mathcal{N}$, as it is only necessary that $\Phi(\underline{x}^{(k+1)}) < \Phi(\underline{x}^k)$ [21]. In the examples considered in the following, step (4b) has been performed by applying the Broyden–Fletcher–Golfarb–Shanno (BFGS) quasi-Newton technique.

The above formulation is completely general and flexible, and takes into account points 1) and 3) considered in the Introduction. In order to answer point 2), it is now obvious that we must look for a state-space with minimal dimensionality, i.e., N should coincide with the *number of degrees of freedom* of the fields radiated by the class of sources considered. In other

words, we must adopt a *nonredundant* field representation. In the next section, we show how this goal can be achieved.

III. Optimal Field Representation in NF–FF Transformation

As stressed in previous sections, the choice of the representation for the field is a key point for managing ill conditioning and trapping problems. This representation should satisfy the following requirements.

1) It should be an *accurate* (within the measurement error) and *efficient* finite-dimensional approximation of the field in the region of interest.
2) For a given accuracy (matching the measurement error) in a given observation region, it should exploit the minimum possible *number of independent parameters* (i.e., of unknowns).
3) The relationship between the independent parameters involved in the representation and the quantities of interest (i.e., the operators $\underline{\mathcal{T}}_{1,2,\infty}$ of Section II) should be as simple as possible in order to easily enforce any a priori information available on the radiated field behavior and reduce the computational effort.

Concerning point 1), it is clear that the representation accuracy must be not lower than the precision of the data. However, a representation which is too accurate is not advisable, since it causes an enlargement of the "space of unknowns," which increases ill conditioning and makes the trapping problem more difficult. This leads to point 2), i.e., the use of a nonredundant representation.

The possibility of reducing the dimensions of the "space of unknowns" for a given representation error depends on the amount of *a priori* information that one is able to introduce in the representation itself. As a matter of fact, any knowledge about the source such as its size and shape, can be used to decrease the number of unknowns. As an example, for an arbitrary array antenna, an optimal representation of the radiated field would exploit the excitation coefficients as unknowns. On the other side, if the array is known in advance to be a focusing one, a representation based on the far-field samples could be more advisable.

Concerning point 3), the possibility of an effective answer is strictly related to the geometries of the source and of the scanning surfaces. For instance, in the case of an (equispaced) planar array, if the excitation coefficients are assumed as unknowns, the operators $\underline{\mathcal{T}}_{1,2,\infty}$ basically become squared Fourier transforms so that they can be efficiently evaluated via a fast Fourier transform(FFT). In light of the above considerations, it can be said that the choice of the state-space is by no means trivial and involves the available *a priori* information.

In order to maintain a sufficient level of generality, we assume that only the geometrical characteristics of the antenna under test, i.e., its location, general shape, and size are known in advance. Efficient and nonredundant field representations over essentially arbitrary surfaces that exploit such information, matching the requirements considered above, have been recently introduced [18], [19]. Such representations are based on the quasi-bandlimitedness property of radiated fields [23].

This band limitation property means that the "reduced" field $\underline{\mathcal{E}} = \underline{E}e^{j\gamma}$, where γ is a properly chosen phase function, and can be closely approximated by a bandlimited function, provided that the bandwidth w, for example, exceeds a critical value W (the field effective bandwidth). The approximation error decreases more than exponentially so that an excess bandwidth factor $\mathcal{X} = w/W$, which is slightly larger than one, ensures an effective control of the approximation error. The bandlimited nature of the reduced field allows us to represent the field along any scanning line by means of cardinal sampling series or more sophisticated central interpolation schemes [18]. An optimal choice of the curve parameterization makes it possible to minimize the number of samples for a given representation error.

By applying this representation to a suitable family of coordinate lines covering the scanning surface, a sampling series representation over the full surface is obtained. The total number of required samples is *finite*, and *independent* of the considered surface, provided that it encloses the source and lies some wavelengths away from it. Furthermore, the interpolation functions, which allow us to evaluate the field from its samples, are *independent* of the shape and location of the source and of the chosen surface which only influence the phase function γ and the optimal parameterization of the coordinate lines. Because the field outside the source is uniquely determined by its tangential components over any enclosing surface,[3] their values at the sampling points can be conveniently assumed as unknowns. Moreover, the freedom in the choice of the surface can be exploited to match the available *a priori* information concerning the field behavior. As an example, when the field can be considered vanishingly small outside the measurement region Σ_1, it is convenient to assume as unknowns the samples located on the surface S_1. In fact, by setting equal to zero all the samples falling outside Σ_1 the *a priori* information is easily taken into account. On the other hand, if the surface moves to infinity, the unknowns become the far-field samples, and the *a priori* knowledge on the focusing nature of the antenna is easily introduced into the field representation.

According to these considerations, we can state that the above sampling series provide effective nonredundant field representations, which make it possible to handle in a natural way the *a priori* information involving either the *far field* or the *near field*.

Explicit expressions for the optimal parameterizations, phase functions and the corresponding sampling rates are available for the main scanning geometries (plane polar, cylindrical, spherical, bi-polar, spiral), as well as for various kind of convex source geometries [18]. A detailed procedure for obtaining representations on generic surfaces is reported in [19].

In the case of a planar source enclosed in a circle of radius a, and a plane-polar scanning geometry (see Fig. 2), as

[3] Note explicitly that no substantial ill conditioning is introduced by "back propagation", as long as we stay some wavelengths by the (nonsuperdirective) source.

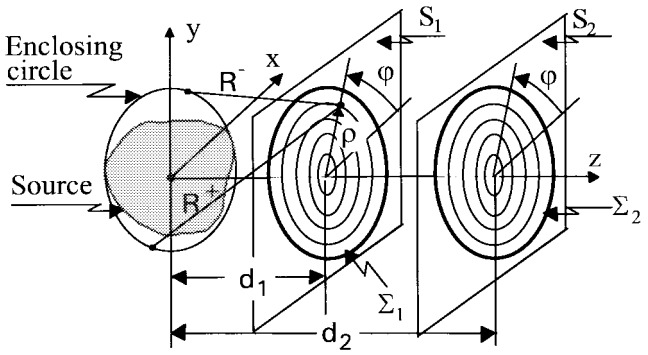

Fig. 2. Plane-polar scanning geometry.

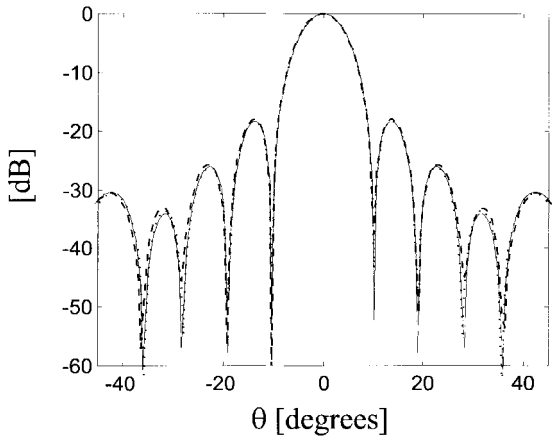

Fig. 3. E-plane copolar far-field amplitude. Continuous line: exact far-field; dotted line: far field from noiseless complex data; dashed line: far field from noiseless intensity data.

considered in the numerical examples reported in the following section, we have [18] $\gamma = \beta(R^+ - R^-)/2$, the optimal coordinate along the circles is the azimuthal angle φ, whereas it is given by $\xi = (R^+ - R^-)/2a$ along the radial lines, and $R^{\pm} = \sqrt{(\rho \pm a)^2 + d^2}$ is the extremal distances from the observation point to the circumference enclosing the source (Fig. 2).

According to [18], when exploiting a canonical sampling series, the field on a point of the observation plane is given by

$$\underline{E}(\xi,\varphi) = \sum_{n} \sum_{\ell=-L_n+1}^{L_n} \underline{E}(\xi_n,\varphi_{n\ell}) e^{j[\gamma(\xi_n)-\gamma(\xi)]} \times \operatorname{sinc}[\pi/\Delta\xi(\xi-\xi_n)] D_{L_n}(\varphi - \ell\Delta\varphi_n) \quad (5)$$

where $\xi_n = n\Delta\xi$, $\Delta\xi = \pi/(\mathcal{X}\beta a)$, $\operatorname{sinc}(x) = \sin(x)/x$, the summation index n is extended to all relevant samples and D_L is the Dirichlet polynomial of degree L, i.e.,

$$D_L(\varphi) = \sin[(2L+1)/2]/[(2L+1)\sin(\varphi/2)] \quad (6)$$

and $\Delta\varphi_n = 2\pi/(2L_n+1)$; $L_n = \operatorname{Int}(\mathcal{X}^*\beta a n \Delta\xi)$ being $\mathcal{X}^* = 1 + (\mathcal{X}-1)\sin^{-2/3}(\xi)$.

IV. Numerical Examples

In order to show the effectiveness of the approach presented, let us consider a planar array of 149 $\lambda/2$ equispaced y-directed, electric dipoles enclosed in a circle with radius 3.5λ and fed by a constant unit current. Two measurement planes S_1 and S_2, with $d_1 = 4\lambda$ and $d_2 = 8\lambda$, respectively (Fig. 2), and a planar scanning geometry are considered. Measurements of the squared amplitude of the y component of the field on each plane have been numerically simulated on a set of 71×71 points located on a $\lambda/4$ regular rectangular mesh $17.5\lambda \times 17.5\lambda$ wide.

According to the considerations made in Section III, since the number of samples is practically independent of the choice of the surface, it is quite natural to assume as unknowns the samples on one of the two measurement planes. The vector $\underline{x}$ should include all samples on that plane, i.e., also those falling outside the scanning area. However, due to the lack of information outside such area, this choice can substantially increase the ill conditioning of the problem and further *a priori* information (for instance on the behavior of the field outside the scanning areas Σ_1 and Σ_2 or also on other surfaces) must be included. When the samples outside the first measurement region can be assumed to be vanishingly small, a computational simple and stable approach (adopted in our numerical analysis) is obtained by setting equal to zero the samples falling outside the scanning area. Then, it is quite natural to choose as unknowns the samples falling on the first plane. However, it must be stressed that in the case of different sources (i.e., highly focusing ones) and different available *a priori* information, other choices of unknowns may be more advisable.

According to these considerations, the vector $\underline{x}$ is assumed to be given by the (complex) samples of the field on the first scanning area at the sampling points $(n\Delta\xi, m\Delta\varphi_n)$ considered in Section III, with an oversampling factor $\mathcal{X} = 1.2$, which ensures a band-limitation error lower than -50 dB.

In order to drive the minimization algorithm (4) to the global minimum of the objective functional (2) the number of unknowns is progressively enlarged. This is performed by retaining only the samples whose amplitude (normalized to the maximum value of the field intensity on Σ_1) is higher than $-Q$ dB, with $Q = 6$, 15, 40, and ∞. For each Q the objective functional (2) is minimized and the result obtained is taken as the starting point for applying the iterative algorithm to the subsequent value of Q. In the last steps, all the unknowns are considered. For the first value of Q, because no *a priori* information involving the phase of the measured field is available, the starting vector $\underline{x}^{(0)}$ of the iterative procedure (4) is obtained by attaching a random phase distribution to the measured amplitudes of the field on Σ_1.

Let us first considered noise-free data. The exact copolar far field on the E-plane, the one evaluated by applying the presented approach and the one obtained by exploiting the simulated near-field complex values inside Σ_1 are reported in Fig. 3 as a continuous, dashed, and dotted line, respectively. The plots show an accurate reconstruction of the far-field from amplitude only near-field data. In fact, the results obtained are almost equal to the one obtained by exploiting the simulated complex near-field falling in the same measurement area on the first plane.

The far-field mean-square error (MSE) due to the truncation error from intensity data is -31.5 dB, while the MSE

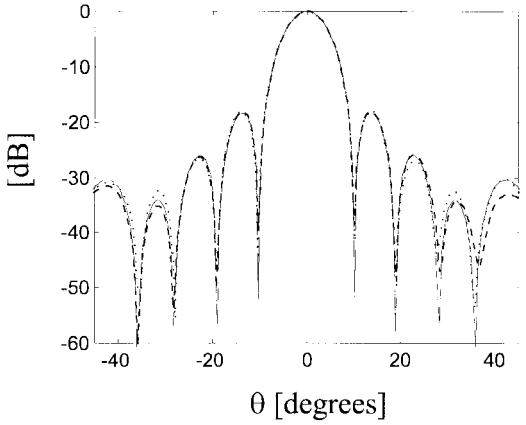

Fig. 4. E-plane copolar far-field amplitude. Continuous line: exact far-field; dotted line: far field from noisy complex data; dashed line: far field from noisy intensity data (noise level $= -35$ dB).

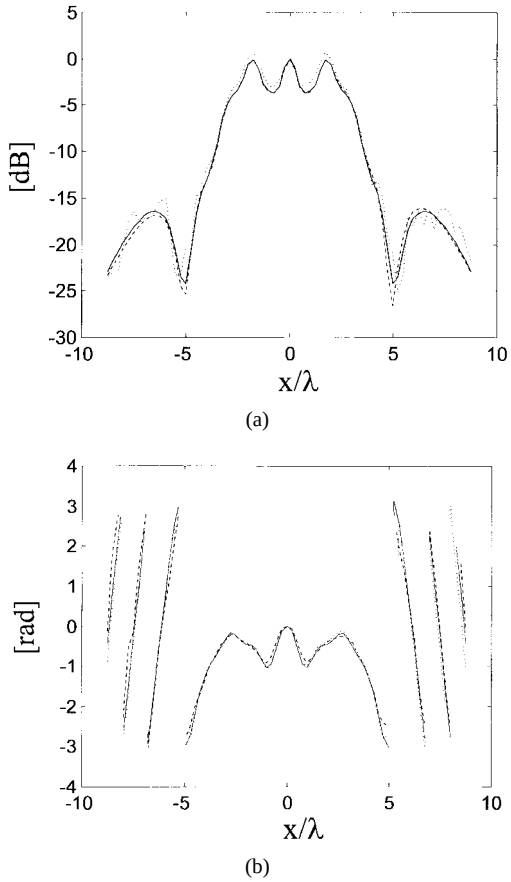

Fig. 5. (a) Near-field y-component intensity along the $y = 0$ axis on Σ_1; continuous line: exact value; dotted line: noisy data; dashed line: near-field amplitude retrieved from noisy intensity data. (b) Near-field y-component phase along the $y = 0$ axis on Σ_1; continuous line: exact value; dotted line: noisy data; dashed line: near-field phase retrieved from noisy intensity data.

from amplitude and phase near-field data is -37.4 dB. The algorithm has been checked considering also smaller scanning areas. For instance, in case of a $12\lambda \times 12\lambda$ scanning area, the MSE from intensity data is -22.7 dB, against -27.9 dB from amplitude and phase data. In the case of a $8\lambda \times 8\lambda$ scanning area, the MSE from intensity data is -13.1 dB, against -19.1 dB from amplitude and phase data, showing the stability of the algorithm respect to the truncation of the near-field data.

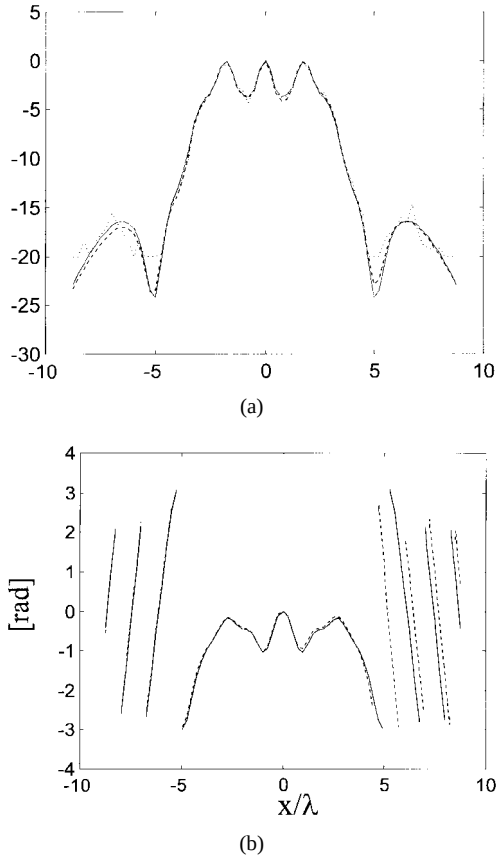

Fig. 6. (a) Near-field y-component amplitude along the $y = 0$ axis on Σ_1; continuous line: exact value; dotted line: noisy and clipped data; dashed line: near-field amplitude retrieved from clipped, noisy intensity data. (b) Near-field y-component phase along the $y = 0$ axis on Σ_1; continuous line: exact value; dashed line: near-field phase retrieved from clipped, noisy intensity data.

In order to check the stability of the algorithm with respect to the noise, the data of the previous example have been corrupted by a white Gaussian noise with an S/N ratio equal to 35 dB. In this case, the *a priori* information concerning the noise level has been taken into account by means of the projectors onto $\mathcal{M}_1$ and $\mathcal{M}_2$. The results obtained concerning the copolar far-field in the E-plane are shown in Fig. 4 where the meaning of the graphs is the same as before. The noiseless amplitude and phase of the near-field y-component, the noisy ones and the corresponding reconstructed ones on the first plane, are shown in Fig. 5(a) (amplitude) and (b) (phase) by continuous, dotted, and dashed lines, respectively. It is noted that the algorithm is able to reconstruct *both the amplitude* and phase of the near field with good accuracy, showing not only good stability with respect to noise, but also some filtering properties. In fact, the noise power falling outside the spatial bandwidth of the field is filtered out in a natural way by the adopted sampling (i.e., bandlimited) representation of the field.

As a last example exploiting numerically simulated data, a noisy measurement system with a low dynamic range has been simulated. Due to the new development of amplitude-only measurement systems exploiting a thermal map of the field [24], this case is of great interest.

Low dynamic noisy data with $S/N = 35$-dB and 20-dB dynamic range were considered. The exact amplitude

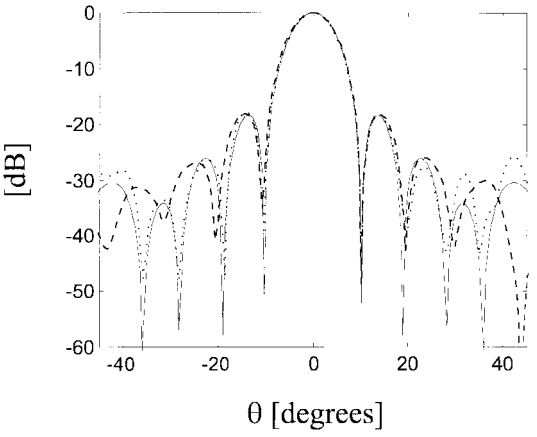

(a)

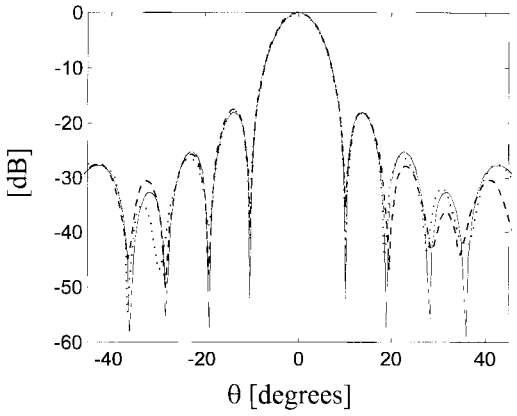

(b)

Fig. 7. (a) E-plane copolar far-field amplitude. Continuous line: exact far field; dotted line: far field from noisy, clipped complex data; dashed line: far field from clipped, noisy intensity data. (b) H-plane copolar far field amplitude. Continuous line: exact far-field; dotted line: far field from noisy, clipped complex data; dashed line: far field from clipped, noisy intensity data.

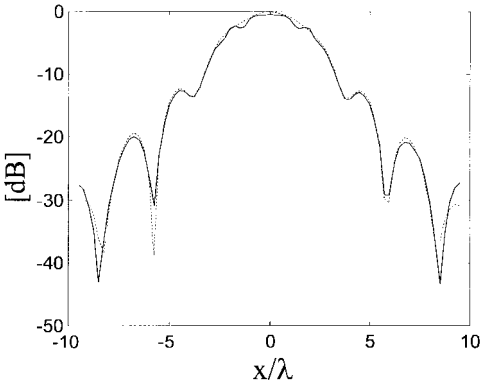

(a)

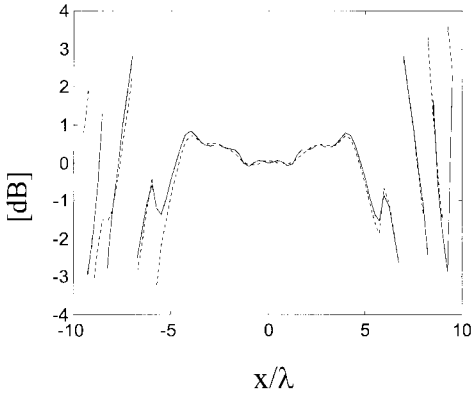

(b)

Fig. 8. (a) Probe-voltage amplitude along the $y = 0$ axis on the surface Σ_1; continuous line: measured value; dashed line: near-field amplitude retrieved from intensity data. (b) Probe-voltage phase along the $y = 0$ axis on the surface Σ_1; continuous line: measured value; dashed line: near-field phase retrieved from intensity data.

(continuous line) of the y-component of the near field along the $y = 0$ axis on the surface Σ_1, the measured one (dotted line) and the one obtained from the phase retrieval procedure (dashed line) are shown under Fig. 6(a), while Fig. 6(b) shows the phase value. The exact copolar far field on the E-plane, the one evaluated by applying the presented approach and the one obtained by exploiting the truncated near-field complex values inside Σ_1 are reported in Fig. 7(a) as a continuous, dashed, and dotted line, respectively. The copolar far-field relative to the H-plane is shown under Fig. 7(b).

Finally, the technique was experimentally validated by exploiting the near-field data collected by a very low-cost facility available at our Microwave Laboratory.[1]

The antenna under test is an in-focus fed parabolic reflector, working at 10 Ghz, with a circular aperture whose radius is equal to 13.5 cm. The field was collected on two surfaces at $d_1 = 7\lambda$ and $d_2 = 14\lambda$ on a grid of 77×77 $\lambda/4$ spaced points by using a small horn probe. No probe correction has been applied.

[1]Dipartimento di Ingegneria Elettronica e della Telecommunicazioni, University di Napoli, Napoli, Italy

The amplitude and the phase of the measured and retrieved probe voltage along the x axis of Σ_1 are shown under Fig. 8(a) and (b) as a continuous and dashed line, respectively. The phase was retrieved considering the nonredundant samples on the first surface as unknowns and assuming $\mathcal{X} = 1.2$. The adopted value of $\mathcal{X}$ ensures a representation error lower than the overall measurement one due to environmental noise, equipment noise and positioning error (estimated to be lower than -45 dB). The resulting number of samples on the full plane at $d_1 = 7\lambda$ is 381, while only 257 of them fall inside the scanning area and are the unknowns of the problem.

The starting point $\underline{x}^{(0)}$ has been chosen randomly as in the previous examples.

Minimization is performed by increasing the value of Q according to the sequence $Q = 6, 15, 30, 45$. A standard NF–FF algorithm is applied to the (complex) data measured on the surface Σ_1 in order to obtain a "reference" copolar far-field whose amplitude on the E- and H-planes as a continuous line is shown under Fig. 9(a) and (b), respectively. The same figures show the copolar far-field amplitude on the same planes, which is obtained by applying the presented approach.

V. Conclusion

A new general and flexible approach to far-field estimation from near-field intensity data has been presented. As it was

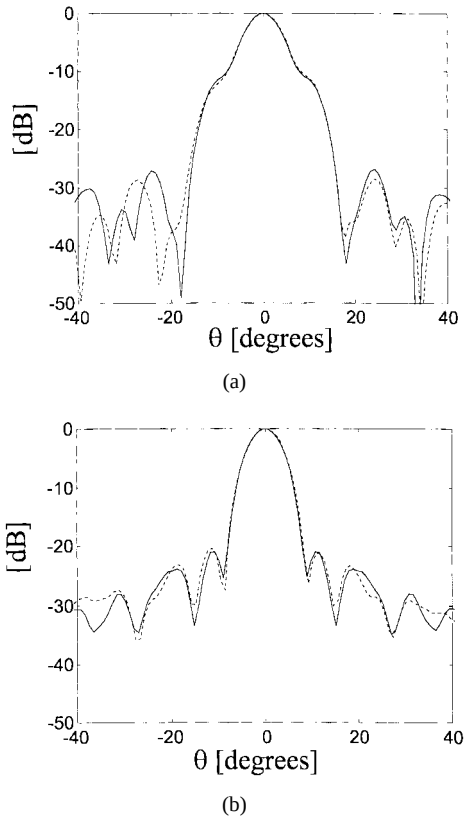

Fig. 9. (a) E-plane copolar far-field amplitude. Continuous line: far field from complex measured data; dashed line: far-field estimated from intensity measured data. (b) H-plane copolar far-field amplitude; continuous line: far field from complex measured data; dashed line: far-field from intensity measured data.

possible to take into account all the available *a priori* information and use a nonredundant representation for the field, this approach can effectively manage ill conditioning and trapping problems typical of the nonlinear inverse problem at hand.

Numerical examples confirm the flexibility and effectiveness of the algorithm and its good performance, even in presence of noisy data and/or low dynamic range. The approach has been also experimentally validated by using a very low-cost measurement system available at our laboratory.

APPENDIX

Considering the projector P_1 expressed as $P_1\underline{y}_1 = (P_{1\mathrm{co}}y_{1\mathrm{co}}, P_{1\mathrm{cr}}y_{1\mathrm{cr}})$, we must evaluate $P_{1\mathrm{co}}y_{1\mathrm{co}}$ and $P_{1\mathrm{cr}}y_{1\mathrm{cr}}$. A point inside Σ_1, $P_{1\mathrm{co}}y_{1\mathrm{co}}$, is given by (A.1) at the bottom of this page. The evaluation of $P_{1\mathrm{co}}y_{1\mathrm{co}}$ at points outside Σ_1 depends on the available a priori information concerning the behavior of the field outside Σ_1. For instance, when we know the ratio, r_{01} for instance, of the power radiated outside Σ_1 to the one radiated inside Σ_1 and the copolar component is much larger than the cross-polar one, we have

$$P_1 y_{1\mathrm{co}} = \begin{cases} y_{1\mathrm{co}} r_{01}/r_1, & \text{outside } \Sigma_1 \\ y_{1\mathrm{co}}, & \text{on } \Sigma_1 \end{cases} \tag{A.2}$$

where r_1 is the power ratio associated to the function to be projected. As a further example, when an upper bound $\bar{m}$ to the squared amplitude of the field outside Σ_1 is known, we have

$$P_{1\mathrm{co}}y_{1\mathrm{co}} \begin{cases} \bar{m}_1, & \text{when } y_{1\mathrm{co}} > \bar{m}_1, \\ y_{1\mathrm{co}}, & \text{when } y_{1\mathrm{co}} < \bar{m}_1. \end{cases} \tag{A.3}$$

The same considerations also apply to the evaluation of the projector $P_{1\mathrm{cr}}y_{1\mathrm{cr}}$.

The evaluation of the projectors $P_2\underline{y}_2$ and $P_\infty\underline{y}_\infty$ can be performed in a very similar way.

REFERENCES

[1] J. Appel-Hansen, "Near-field far-field antenna measurements," in *Antenna Handbook*, Y. T. Lo, Ed., New York: Van Nostrand Reinhold, 1988, ch. 33, pp. 1–31.
[2] A. D. Yaghijian, "An overview of near-field antenna measurements," *IEEE Trans. Antennas Propagat.*, vol. AP-34, pp. 30–45, June 1986.
[3] "Special issue on near-field scanning techniques," *IEEE Trans. Antennas Propagat*, vol. 36, pp. 725–301, June 1988.
[4] L. I. Williams, Y. Rahmat-Samii, and R. G. Yaccarino, "The bi-polar planar near-field measurement technique—Part I: Implementation and measurement comparison," *IEEE Trans. Antennas Propagat.*, vol. 42, pp. 184–195, Feb. 1994.
[5] O. M. Bucci and G. D'Elia, "A new near-field sampling representation from samples on planar spiral," in *Proc. Antennas Propagat. Soc.*, Montreal, Canada, pp. 176–179, July 1997.
[6] L. I. Williams, R. G. Yaccarino, and Y. Rahmat-Samii, "Polar thinned-polar, and linear spiral sampling using the UCLA bi-polar planar near-field measurement system: A comparative study," in *Proc. 1994 IEEE Antennas Propagat. Soc. Symp.*, Seattle, WA, July 1994, pp. 548–561.
[7] G. Junkin, T. Huang, and J. C. Bennett, "Holographic near-field/far-field for terahertz antenna testng," in *Proc. Antenna Measurement Techniques Assoc. Conf.*, Boston, MA, Nov. 1997, pp. 419–424.
[8] A. P. Anderson and S. Sali, "New possibilities for phaseless microwave diagnostics—Part I: Error reduction techniques," *Proc. Inst. Elect. Eng.*, vol 132, pt. H, pp. 291–298, 1985.
[9] O. M. Bucci, G. D'Elia, G. Leone, and R. Pierri, "Far-field pattern determination from the near-field amplitude on two surfaces," *IEEE Trans. Antennas Propagat*, vol. 38, pp. 1772–1779, Nov. 1990.
[10] V. Yu Ivanov, V. P. Sivokon, and M. A. Vorontsov, "Phase retrieval from a set of intensity measurements: Theory and experiment," *J. Opt. Soc. Amer.*, vol. A9, pp. 1515–1524, 1992.
[11] R. G. Yaccarino and Y. Rahmat-Samii, "Phaseless bi-polar near-field measurements: A squared amplitude interpolation iterative fourier algorithm," in *17th Annu. Antenna Meas. Tech. Assoc. Symp. Dig.*, Williamsburg, VA, Nov. 1995, pp. 195–200.
[12] T. Isernia, G. Leone, and R. Pierri, "Radiation pattern evaluation from near-field intensities on planes," *IEEE Trans, Antennas Propagat*, vol. 44, pp. 701–710, May 1996.
[13] L. S. Taylor, "The phase retrieval problem," *IEEE Trans. Antennas Propagat.*, vol. AP-29, pp. 386–391, Mar. 1981.

$$P_{1\mathrm{co}}y_{1\mathrm{co}} = \left.\begin{cases} \widehat{M}^2_{1\mathrm{co}} - \varepsilon_1, & \text{when } y_{1\mathrm{co}} < \widehat{M}^2_{1\mathrm{co}} - \varepsilon_1 \\ \widehat{M}^2_{1\mathrm{co}} + \varepsilon_1, & \text{when } y_{1\mathrm{co}} > \widehat{M}^2_{1\mathrm{co}} + \varepsilon_1 \\ y_{1\mathrm{co}}, & \text{when } \widehat{M}^2_{1\mathrm{co}} - \varepsilon_1 \le y_{1\mathrm{co}} \le \widehat{M}^2_{1\mathrm{co}} + \varepsilon_1 \\ 10^{-d_r/10}, & \text{if } [\max(y_{1\mathrm{co}})]_{\mathrm{dB}} - [y_{1\mathrm{co}}]_{\mathrm{dB}} > d_r \end{cases}\right\} \text{if } [\max(y_{1\mathrm{co}})]_{\mathrm{dB}} - [y_{1\mathrm{co}}]_{\mathrm{dB}} < d_r \tag{A.1}$$

[14] R. J. Fienup, "Phase retrieval algorithms: A comparison," *Appl. Opt.*, vol. 21, pp. 2758–2769, Aug. 1982.
[15] P. J. van Laarhoven and E. H. L. Aarts, *Simulated Annealing: Theory and Applications*. Norwell, MA: Kluwer, 1998.
[16] T. Back, D. B. Fagel, and Z. Michalewicz (Eds.), *Handbook of Evolutionary Computation*. London, U.K.: Oxford Univ. Press, 1997.
[17] O. M. Bucci, A. Capozzoli, and G. D'Elia, "A hybrid evolutionary algorithm in the diagnosis of reflector distorsions," in *Proc. 10th JINA*, Nice, France, Nov. 1998, pp. 513–516.
[18] O. M. Bucci and G. D'Elia, "Advanced sampling techniques in electromagnetics," *The Review of Radio Science 1993–1996*, W. R. Stone, Ed. London, U.K.: Oxford Univ. Press, 1996.
[19] O. M. Bucci, C. Gennarelli, and C. Savarese, "Representation of electromagnetic fields over arbitrary surfaces by a finite and nonredundant number of samples," *IEEE Trans. Antennas Propagat.*, vol. 46, pp. 351–359, Mar. 1998.
[20] W.-X. Cong, N.-X. Chen, and B.-Y. Gu, "Phase retrieval in the fresnel transform system: A recursive algorithm," in *Signal Recovery Synthesis Tech. Digest, Proc. Opt. Soc. Amer. Symp.*, Kailua-Kone, HI, July 1998, pp. 55–57.
[21] O. M. Bucci, G. D'Elia, G. Mazzarella, and G. Panariello, "Antenna pattern synthesis: A new general approach," *Proc. IEEE*, vol. 82, pp. 358–371, Mar. 1994.
[22] O. M. Bucci and G. Franceschetti, "On the degrees of freedom of scattered fields," *IEEE Trans. Antennas Propagat.*, vol. 37, pp. 918–926, July 1989.
[23] _____, "On the spatial bandwidth of scattered fields," *IEEE Trans. Antennas Propagat.*, vol. AP-35, pp. 1445–1455, Dec. 1987.
[24] J. E. Will, J. D. Norgard, M. Seifert, A. Pesta, J. Cleary, C. F. Stubenrauch, and K. MacReynolds, "Antenna near field phase data from infrared thermograms by fourier iterative plane-to-plane techniques," in *Proc. Antenna Measurement Techniques Assoc. Conf.*, Seattle, WA, 1996, pp. 198–203.

Ovidio M. Bucci (SM'82–F'93), for a photograph and biography, see p. 994 of the June 1997 issue of this TRANSACTIONS.

Giuseppe D'Elia, for a photograph and biography, see p. 1225 of the November 1995 issue of this TRANSACTIONS.

Marco Donald Migliore, for a photograph and biography, see p. 994 of the June 1997 issue of this TRANSACTIONS.